Structural and Electronic Properties of *T* Graphene: A Two-Dimensional Carbon Allotrope with Tetrarings

Yu Liu, Gang Wang,* Qingsong Huang, Liwei Guo, and Xiaolong Chen†

Research & Development Center for Functional Crystals, Beijing National Laboratory for Condensed Matter Physics, Institute of Physics, Chinese Academy of Sciences, Beijing 100190, China

(Received 3 May 2011; revised manuscript received 14 January 2012; published 31 May 2012)

T graphene, a two-dimensional carbon allotrope with tetrarings, is investigated by first-principles calculations. We demonstrate that buckled *T* graphene has Dirac-like fermions and a high Fermi velocity similar to graphene even though it has nonequivalent bonds and possesses no hexagonal honeycomb structure. New features of the linear dispersions that are different from graphene are revealed. π and π^* bands and the two comprising sublattices are the key factors for the emergence of Dirac-like fermions. *T* graphene and its two types of nanoribbon are expected to possess additional properties over graphene due to its different band structure.

DOI: 10.1103/PhysRevLett.108.225505 PACS numbers: 61.48.−c, 71.15.Mb, 73.22.−f

The amazing two-dimensional (2D) carbon allotrope, graphene, reveals a number of unique properties, such as the half-integer quantum Hall effect, the never falling conductivity, and massless carriers [1]. These electronic properties arise from its linear dispersion relation around the crossing point (the Dirac point) of two opposite cones at *K* point in the band structure (BS) due to the graphene's crystal symmetry. Its honeycomb lattice consisting of two equivalent carbon sublattices plays a crucial role in forming such an intriguing BS [2]. Under this crystal symmetry, different sublattices contribute the electronic states near the zero energy and make the holes and electrons conjugated. So carriers in graphene can be described by the Dirac equations and are called Dirac fermions. Enyashin and Ivanovskii [3] constructed 12 artificial 2D carbon networks with varying hybridizations among carbons and examined their stability and electron structures. They found a network with hexagonal cell exhibiting a graphenelike electronic behavior. Silicene was predicted to possess a similar BS and Dirac-like fermions and then experimentally observed [4,5]. A recent study, however, showed that Dirac fermions can persist in the strained graphene without a regular hexagonal symmetry [6], implying a hexagonal lattice is not an indispensable condition whereby Dirac fermions exist. Then a question arises: is it possible for a 2D carbon lattice with different symmetry to exhibit similar properties? If so, what are the determining factors?

Then we try to construct a 2D carbon sheet with tetragonal symmetry while considering its feasibility to obtain it by experiment. We notice that cubic and tetragonal carbon lattices are known to exist in some carbon allotropes, such as body-centered cubic (bcc) C_8 [7–9] and body-centered tetragonal (bct) C_4 [10–13] as shown in Fig. 1(a) and 1(b). These materials draw attention due to their superhard properties. Bcc C_8 prepared by plasma deposition [7] or pulsed-laser induced liquid-solid interface reaction [9] is thought to be denser (4.1 g/cm^3) than diamond (3.51 g/cm^3) and has an indirect band gap of about 5.5 eV [8]. It consists of C_8 cubes with a lattice constant of 4.28 Å. Superhard bct C_4 with an indirect band gap of 3.78 eV, which probably exists in cold-compressed graphite, consists of carbon tetrarings with lattice constants $a =$ 4.33 Å, $c = 2.48$ Å [11].

In this Letter, we investigate the structural and electronic properties of a 2D tetrasymmetrical carbon named *T* graphene using the first-principles calculations. *T* graphene could be considered to be derived from cleaving two adjacent atom layers in bcc C_8 or bct C_4 along (001). We demonstrate that this carbon allotrope can be energetically metastable and dynamically stable. It is found that *T* graphene has Dirac-like fermions and a high Fermi velocity though it has nonequivalent (two kinds) bonds and nonhoneycomb structure. Dirac-like fermions actually arise from the crossing π and π^* bands and two sublattices, whereas hexrings are actually not necessary. Furthermore, the crossing points are not only at *K* points as in graphene, but form a loop with tetrasymmetry in Brillouin zone. The properties of *T* graphene nanoribbons (TGNRs) and strained *T* graphene are also investigated.

The first-principles calculations were based on density functional theory with generalized gradient approximation (GGA) in the form of Perdew-Burke-Ernzerhof function [14] for exchange-correlation potential. All the calculations were performed using the Cambridge Serial Total Energy Package [15], which has been proved to be workable to understand the experimental phenomena in graphene [16]. The vacuum slabs of 10 Å were used to avoid interactions between adjacent atom layers. A self-consistent field method (tolerance 5.0×10^{-7} eV/atom) was employed in conjunction with plane-wave basis sets of cutoff energy of 660 eV using ultrasoft pseudopotentials [17] in reciprocal space. Geometry optimization was implemented until the remanent Hellmann-Feynman forces

on the ions were less than 0.01 eV/Å. The first Brillouin zone was sampled with grid spacing of 0.04 $Å^{-1}$ for wave functions and 0.01 $Å^{-1}$ for the density of states (DOS) on the basis of Monkhorst-Pack special k-point scheme [18]. Phonon dispersion relations were obtained with the finite displacement method. We checked the convergence of the phonon spectra and found the phonon frequencies vary within 1% if the supercell contains four neighbors or more [19]. Free energies as a function of temperature were performed by using phonon dispersion with the quasiharmonic approximation [19,20]. We further examined the stability of the structures performing first-principles finite temperature molecular dynamics (MD) simulations by using time steps of 1 femtosecond in 4×4 supercells.

We considered planar T graphene and buckled T graphene as shown in Fig. 1(c) and 1(d). Planar T graphene is ideally 2D and has one sublattice in the unit cell, which is similar to the model 7 proposed in [3]. If two adjacent square lattices are not in the same height along the Z axis, it becomes buckled T graphene, which possesses two interpenetrating square sublattices. Planar T graphene after geometry optimization can be described by the plane group $p4mm$ with a lattice constant 3.42 Å containing four atoms in each cell, close to the value (3.47 Å) of the model 7 in [3]. Buckled T graphene of the plane group $p4mm$ has a lattice constant 4.84 Å and an equilibrium height difference (Δz) of about 0.55 Å between two nearest-neighbor tetrarings. We calculated the formation energies of different carbon allotropes in order to understand the stability of T graphene. The GGA approximation has been proven to be reliable in calculating the formation energies of carbon allotropes [21]. We checked and confirmed the precision of these calculations is satisfactory. Among graphene (-9.26 eV/atom), graphite $2H$ (-9.25 eV/atom), diamond (-9.10 eV/atom), bct C_4 (-8.92 eV/atom), bcc C_8 (-8.49 eV/atom), recently synthesized large area graphdiyne [22] (-8.49 eV/atom), and most recently predicted T carbon [21] (-7.95 eV/atom), planar T graphene and buckled T graphene have comparable formation energies -8.73 eV/atom and -8.41 eV/atom respectively, suggesting that T graphene could be thermodynamically metastable. In terms of free energy, as shown in Fig. 1(e), the thermodynamic stability of planar T graphene is better than other allotropes except graphene when the temperature is roughly below 900 K, while buckled T graphene, similar to the T carbon, is more stable when above roughly 940 K. To further confirm the dynamic stability, we calculated the phonon spectra of T graphene. In Fig. 1(f) and 1(g), all their branches have positive frequencies and no imaginary phonon modes in T graphene are found, confirming the dynamic stability of T graphene. MD simulations indicated that planar T graphene and buckled T graphene are not destroyed at 700 K and 500 K in 100 steps and the structures can maintain at 700 K and 500 K for at least 1 picosecond. Silicene and N-doped graphene show similar stability by MD calculations [4,23].

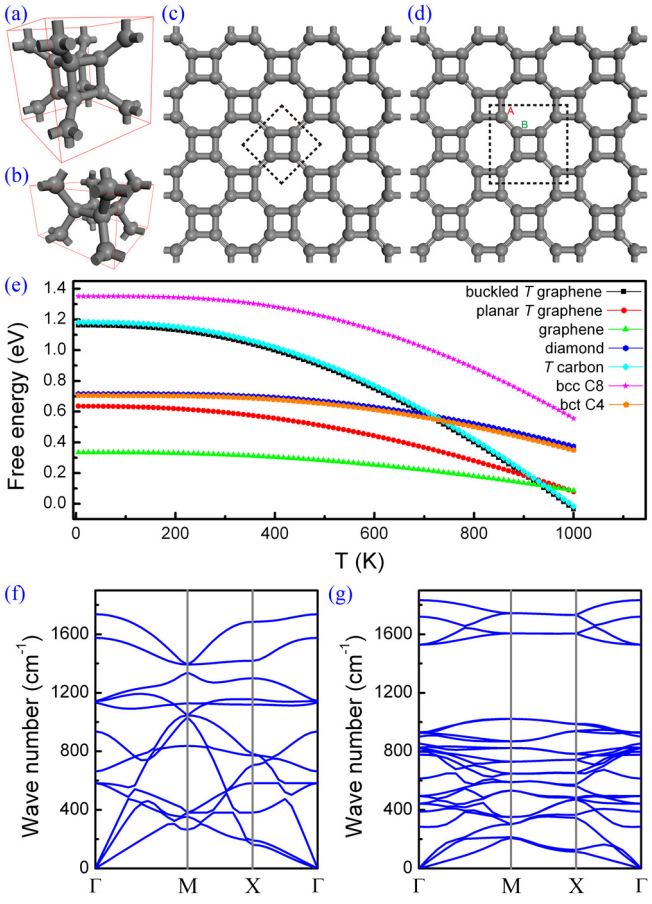

FIG. 1 (color online). (a) (b) The unit cells of bcc C_8 and bct C_4. (c) (d) The structures of planar T graphene and buckled T graphene. (e) Free energies of several carbon allotropes as a function of temperature. (f) (g) The phonon spectra of planar T graphene and buckled T graphene. The black dashed squares suggest unit cells of T graphene. Letters "A" and "B" represent atoms in each sublattice. Gray spheres and sticks represent carbon atoms and bonds, respectively. The locations of points $\Gamma(0, 0)$, $M(0.5, 0.5)$, and $X(0, 0.5)$ are shown in Fig. 3.

BSs and DOS of T graphene are depicted in Fig. 2. The electronic structure shows planar T graphene is metallic, which is agreeable with the previous report [3]. While, the BS of buckled T graphene shows the linear dispersion relation near the Fermi level and two cross points located at asymmetric positions $\Xi(0.170, 0.170)$ between Γ and M and $\Lambda(0, 0.249)$ between X and Γ (fractional coordinates in reciprocal space, similarly hereinafter) under the present calculation accuracy. These two cross points roughly locate at the Fermi level, as the energy levels from the Fermi energy is 0 eV and 25 meV, respectively. Examining states near the Fermi level reveals that the DOS is 1.04 states/eV/cell, which is close to zero. To further understand the distribution of the linear dispersion relation

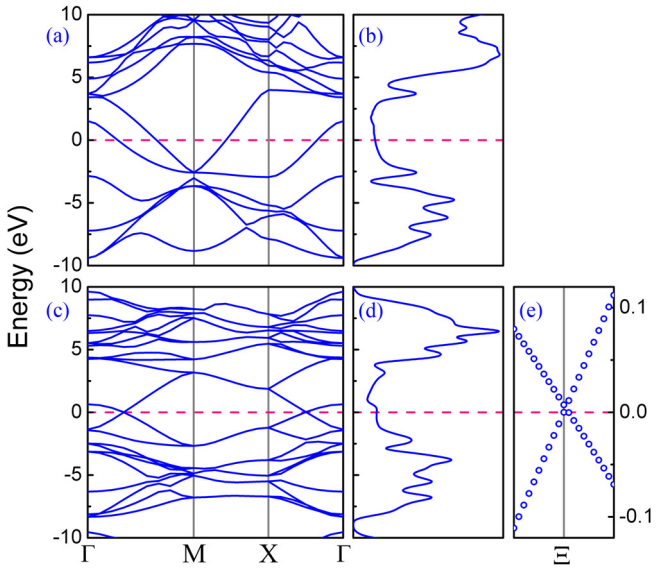

FIG. 2 (color online). The electronic structures of T graphenes. (a) (b) The entire BS and the DOS of planar T graphene. (c) (d) The entire BS and the DOS of buckled T graphene. (e) Amplification of the BS around the Ξ point. The Fermi energy is set to 0 eV, similarly hereinafter.

in reciprocal space, we calculated the BS from Γ to a series of points between X and M. The results indicate that the linear dispersion relation near the Fermi level exists in each direction. As shown in the three-dimensional (3D) BS illustrated in Fig. 3(a) and the magnified one in Fig. 3(b), large quantity of cross points located at asymmetric positions form a loop [see Fig. 3(c)] with tetrasymmetry, leading to the coexistence of near-zero DOS at the Fermi level and the linear dispersion relation in buckled T graphene.

The linear dispersion relation near the Fermi surface with cross points demonstrates that carriers in buckled

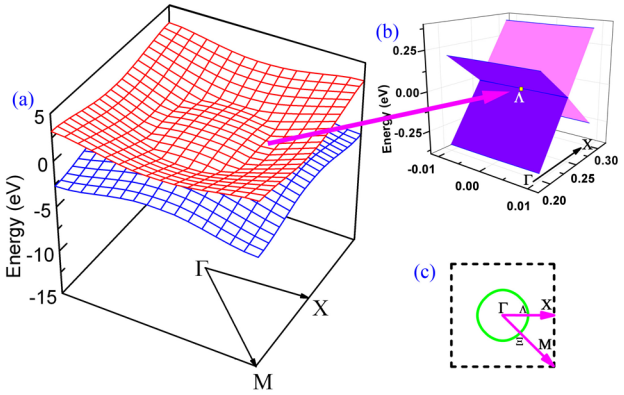

FIG. 3 (color online). (a) The two layers of the 3D BS near the Fermi surface in the first Brillouin zone of T graphene. (b) The magnified 3D BS near the Fermi surface around the Λ point of T graphene ranged in 0.1×0.02. (c) The loop (green solid line) formed by cross points in the first Brillouin zone (black dashed line).

T graphene should be massless and have a Dirac fermion character. If P is a random point on the cross-point loop, the dispersion relation around the P point can be further analyzed by expanding the BS as $\mathbf{k} = \mathbf{P} + \mathbf{q}$, with $|\mathbf{q}| \ll |\mathbf{P}|$, $E_{\pm}(\mathbf{q}) \approx \pm v_F|\mathbf{q}| + O[(|\mathbf{q}|/|\mathbf{P}|)^2]$, where $\mathbf{q}$ is a minor momentum relative to P and v_F is the Fermi velocity. By neglecting the second and higher order terms, the Fermi velocity is estimated to be $\sim 10^6$ m/s according to $v_F \approx E(\mathbf{q})/|\mathbf{q}|$, which is close to the theoretical value of graphene. Buckled T graphene is also ambipolar like graphene because of the electron-hole symmetry at cross points. The DOS of buckled T graphene near the Fermi level brings a carrier concentration as high as 10^{13} cm^{-2} estimated at 300 K, which is similar to that of graphene.

As demonstrated above, buckled T graphene is found to be an ambipolar 2D carbon allotrope with remarkable properties of Dirac-like fermions and a high v_F. For such a sp^2-bonded structure, σ bond is responsible for the formation of the framework. The remained p_z orbital, which is roughly vertical to the tetrarings, binds covalently with each other and forms π bands and π^* bands. These π and π^* bands near the Fermi surface are believed to induce the linear dispersion relation near the Fermi surface. So the emergence of Dirac-like fermions in buckled T graphene is attributed to π and π^* bands, which is similar to that of graphene [2]. However, planar T graphene with π and π^* bands does not have the linear dispersion relation, so π and π^* bands are not sufficient for the emergence of the linear dispersion relation. Two sublattices within one unit cell, which is one of the general characteristics of graphene [2], buckled T graphene, silicene [4], germanene [4], and the strained graphene, is thought to be another important factor for the formation of the linear dispersion relation. In contrast, the planar T graphene has only one sublattice in the unit cell, leading to that the linear dispersion does not persist and its BS becomes metal-like.

It is demonstrated that structure tailoring and mechanical straining induce many new properties in graphene, which are of both fundamental and technological importance. For buckled T graphene, intriguing properties may also arise upon reducing it into nanoribbon and/or applying of strain. The most interesting question is whether TGNRs will open a band gap like graphene nanoribbons or not [24]. If true, the band gap most possibly emerges in armchair TGNR (TGNR-1) with width of only one lattice constant of buckled T graphene ($n = 4$) shown in Fig. 4(a), as TGNR-1 has the strongest quantum confinement effect. While, as shown in Fig. 4(b), it is found that the linear dispersion relation still exists in TGNR-1. Furthermore, zigzaglike TGNR (TGNR-2) ($n = 4$) created by cleaving buckled T graphene along ⟨11⟩ shown in Fig. 4(c) is calculated to have a metallic BS without the linear dispersion relation [see in Fig. 4(d)]. The results demonstrate that structure tailoring without edge decorations cannot open a band gap. The magnetism of

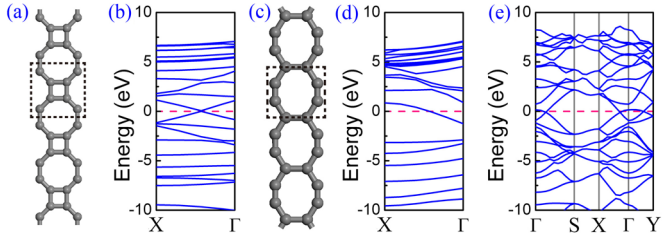

FIG. 4 (color online). (a) (b) The structure and the BS of TGNR-1 ($n = 4$). The black dashed square suggests the unit cell of TGNR. Gray spheres and sticks represent carbon atoms and bonds, respectively. (c) (d) The structure and the BS of TGNR-2 ($n = 4$) from cleaving of buckled T graphene along $\langle 11 \rangle$. (e) The BS of buckled T graphene with 20% extension in length along the X axis.

nanoribbons is another interesting issue. We carried out spin-polarized first-principles calculations and found that TGNR-1 is diamagnetic and TGNR-2 yields 0.038 μB/atom. The energy difference between the antiferromagnetic and ferromagnetic phases is 10.4 meV, so TGNR-2 prefers a ferromagnetic state. This result is similar to zigzag graphene and silicene nanoribbons [4,24] but with stronger coupling while less magnetic moments than zigzag silicene nanoribbons [4]. Figure 4(e) shows the BS of buckled T graphene with extension of 20% along the X axis suggesting that the linear dispersion relation still survives. It indicates that the band gap of buckled T graphene cannot be tuned by introducing planar strains within a certain range. Similar results in graphene were reported by Choi *et al.* [6].

Comparing over graphene, buckled T graphene might possess additional properties to be utilized due to its different BS and its nonstrict 2D properties. For instance, electrons are expected to focus more easily when passing through a p-n junction as predicted for Veslago lens [25]. Since T graphene is buckled, it is helpful to avoid the distortions as in graphene [26] and more uniform properties over the total sheet are expected.

T graphene might be experimentally obtained considering its comparable formation energy and free energy to other existing carbon allotropes and dynamic stability. The recent experimental progresses of relevance are revealing and supportive. For instance, Kotakoski and co-workers [27] obtained a one-dimensional carbon structure consisting alternately of carbon tetrarings and octarings by electron beam irradiating on graphene that much resembles the one predicted type of nanoribbon (TGNR-1). Lahiri and coworkers [28] achieved another 1D structure containing carbon octarings and pentarings by defect engineering, serving another example of the existence of carbon octaring sheet. Here we propose two possible routes. One is to deposit carbon atoms on certain metal substrates, which has been applied in the preparation of graphene [29] and silicene [30]. Strong constraint exerted by metal lattices on carbon atoms may induce the crystallization of tetracarbon lattice. Meanwhile, based on the progresses mentioned above, another route is proposed to combine the tailored graphene growing on Ni (111) and the electron beam irradiation, enabling us to create the carbon tetrarings and octarings first and then to enlarge them into 2D sheets by defect engineering. At the moment, lots of efforts are needed to this end.

In summary, T graphene is theoretically demonstrated to be a 2D carbon allotrope which can be energetically metastable and dynamically stable. Buckled T graphene has Dirac-like fermions and a high v_F similar to graphene though it has nonequivalent (two kinds) bonds and no honeycomblike structure. It is proved that the linear dispersion relation near the Fermi surface exists in every direction and the cross points form a loop. The existence of Dirac-like fermions is attributed to crossing π and π^* bands and two sublattices. Under certain structure tailoring or straining, the linear dispersion relation is found to be retained. TGNR-1 is found to be diamagnetic and TGNR-2 ferromagnetic. Possible preparation routes are also proposed. T graphene actually demonstrates the possible novel materials owning Dirac-like fermions with a tetragonal symmetry. Our study provides some insights to build interesting new 2D carbonic materials with Dirac-like fermions.

Y. Liu would like to thank Y. P. Jia, J. J. Lin, X. Lu, J. S. Liu, and L. D. Pan of Institute of Physics, CAS and S. Chen of Nanjing University for the fruitful discussions. This work was partly supported by the Ministry of Science and Technology of China (Grant No. 2011CB932700), the Chinese Academy of Sciences (Grant No. KJCX2-YW-W22), and the National Natural Science Foundation of China (Grant Nos. 90922037, 51072223, and 50972162).

*gangwang@iphy.ac.cn
†chenx29@iphy.ac.cn

[1] K. S. Novoselov, A. K. Geim, S. V. Morozov, D. Jiang, M. I. Katsnelson, I. V. Grigorieva, S. V. Dubonos, and A. A. Firsov, Nature (London) **438**, 197 (2005).
[2] J. Hass, W. A. de Heer, and E. H. Conrad, J. Phys. Condens. Matter **20**, 323202 (2008).
[3] A. N. Enyashin and A. L. Ivanovskii, Phys. Status Solidi B **248**, 1879 (2011).
[4] S. Cahangirov, M. Topsakal, E. Aktürk, H. Sahin, and S. Ciraci, Phys. Rev. Lett. **102**, 236804 (2009).
[5] P. De Padova, C. Quaresima, C. Ottaviani, P. M. Sheverdyaeva, P. Moras, C. Carbone, D. Topwal, B. Olivieri, A. Kara, H. Oughaddou, B. Aufray, and G. Le Lay, Appl. Phys. Lett. **96**, 261905 (2010).
[6] S. M. Choi, S. H. Jhi, and Y. W. Son, Phys. Rev. B **81**, 081407 (2010).
[7] V. E. Strel'nitskii, V. G. Padalka, and S. I. Vakula, Zh. Tekh. Fiz. **48**, 377 (1978); Sov. Phys. Tech. Phys. **23** 222 (1978).
[8] R. L. Johnston and R. Hoffmann, J. Am. Chem. Soc. **111**, 810 (1989).

[9] P. Liu, H. Cui, and G. W. Yang, Cryst. Growth Des. **8**, 581 (2008).
[10] W. L. Mao, H. K. Mao, P. J. Eng, T. P. Trainor, M. Newville, C. C. Kao, D. L. Heinz, J. F. Shu, Y. Meng, and R. J. Hemley, Science **302**, 425 (2003).
[11] K. Umemoto, R. M. Wentzcovitch, S. Saito, and T. Miyake, Phys. Rev. Lett. **104**, 125504 (2010).
[12] X. F. Zhou, G. R. Qian, X. Dong, L. X. Zhang, Y. J. Tian, and H. T. Wang, Phys. Rev. B **82**, 134126 (2010).
[13] P. Y. Wei, Y. Sun, X. Q. Chen, D. Z. Li, and Y. Y. Li, Appl. Phys. Lett. **97**, 061910 (2010).
[14] J. P. Perdew, K. Burke, and M. Ernzerhof, Phys. Rev. Lett. **77**, 3865 (1996).
[15] S. J. Clark, M. D. Segall, C. J. Pickard, P. J. Hasnip, M. I. J. Probert, K. Refson, and M. C. Payne, Z. Kristallogr. **220**, 567 (2005).
[16] Z. Fei, Y. Shi, L. Pu, F. Gao, Y. Liu, L. Sheng, B. G. Wang, R. Zhang, and Y. D. Zheng, Phys. Rev. B **78**, 201402 (2008).
[17] D. Vanderbilt, Phys. Rev. B **41**, 7892 (1990).
[18] H. J. Monkhorst and J. D. Pack, Phys. Rev. B **13**, 5188 (1976).
[19] N. Mounet and N. Marzari, Phys. Rev. B **71**, 205214 (2005).
[20] K. Reuter and M. Scheffler, Phys. Rev. B **65**, 035406 (2001).
[21] X. L. Sheng, Q. B. Yan, F. Ye, Q. R. Zheng, and G. Su, Phys. Rev. Lett. **106**, 155703 (2011).
[22] G. X. Li, Y. L. Li, H. B. Liu, Y. B. Guo, Y. J. Li, and D. B. Zhu, Chem. Commun. (Cambridge) **46**, 3256 (2010).
[23] H. J. Xiang, B. Huang, Z. Y. Li, S. H. Wei, J. L. Yang, and X. G. Gong, Phys. Rev. X **2**, 011003 (2012).
[24] Y. W. Son, M. L. Cohen, and S. G. Louie, Phys. Rev. Lett. **97**, 216803 (2006).
[25] V. V. Cheianov, V. Fal'ko, and B. L. Altshuler, Science **315**, 1252 (2007).
[26] J. C. Meyer, A. K. Geim, M. I. Katsnelson, K. S. Novoselov, T. J. Booth, and S. Roth, Nature (London) **446**, 60 (2007).
[27] J. Kotakoski, A. V. Krasheninnikov, U. Kaiser, and J. C. Meyer, Phys. Rev. Lett. **106**, 105505 (2011).
[28] J. Lahiri, Y. Lin, P. Bozkurt, I. I. Oleynik, and M. Batzill, Nature Nanotech. **5**, 326 (2010).
[29] Y. Pan, H. G. Zhang, D. X. Shi, J. T. Sun, S. X. Du, F. Liu, and H. J. Gao, Adv. Mater. **21**, 2777 (2009).
[30] A. Kara, C. Léandri, M. E. Dávila, P. De Padova, B. Ealet, H. Oughaddou, B. Aufray, and G. Le Lay, J. Supercond. Novel Magnetism **22**, 259 (2009).